Kinetic Studies on the Reactions of CF_3 with $O(^3P)$ and H Atoms at High Temperatures

Kazuo Takahashi,* Yoshinobu Sekiuji, Yasuyuki Yamamori, and Tadaaki Inomata

Department of Chemistry, Sophia University, 7-1 Kioi-cho, Chiyoda-ku, Tokyo 102-8554, Japan

Keiichi Yokoyama

Japan Atomic Energy Research Institute, Tokai-mura, Ibaraki 319-1195 Japan

Received: April 27, 1998; In Final Form: July 17, 1998

The kinetics of the high-temperature reactions of CF_3 radicals with $O(^3P)$ and H atoms has been investigated experimentally and theoretically. The product channels of the $CF_3 + O(^3P)$ and $CF_3 + H$ reactions were examined by calculating their branching fractions with the multichannel Rice−Ramsperger−Kassel−Marcus (RRKM) theory. Structural parameters, vibrational frequencies, and threshold energy required for the RRKM calculation were obtained from an ab initio MO calculation. The theoretical calculation showed that the productions of $CF_2O + F$ and $CF_2(^1A_1) + HF$ were the unique possible channels for the $CF_3 + O(^3P)$ and $CF_3 + H$ reactions, respectively, and that the other channels such as deactivation were negligible for both the reactions. The rate coefficients for these reactions were experimentally determined by using a shock tube−atomic resonance absorption spectroscopy technique over the temperature ranges of 1900−2330 and 1150−1380 K and the total density ranges of 8.2×10^{18}−1.2×10^{19} and 6.1×10^{18}−9.8×10^{18} molecules·cm^{-3}. Nitrous oxide and ethyl iodide were used as precursors of electronically ground-state oxygen and hydrogen atoms, respectively. Trifluoromethyl radicals were produced through the thermal dissociation of CF_3I. The rate coefficients for the reactions $CF_3 + O(^3P) \rightarrow CF_2O + F$ (1b) and $CF_3 + H \rightarrow CF_2(^1A_1) + HF$ (2c) were obtained from the decay profiles of O- and H-atom concentrations as $k_{1b} = (2.55\pm0.23) \times 10^{-11}$ and $k_{2c} = (8.86\pm0.32) \times 10^{-11}$ cm^3 molecule^{-1} s^{-1} (error limits at the one standard deviation level). Neither rate coefficient had any temperature or pressure dependence under the present experimental conditions; the values were in good agreement with some room-temperature data reported previously.

Introduction

Halons, bromine-containing perhalogenated carbons such as CF_3Br, CF_2BrCl, and $C_2F_4Br_2$, have been used for many years as gaseous fire-extinguishing agents. They have high fire-extinguishing abilities because of their chemical suppression mechanism, that is, bromine-containing species can catalytically remove active species from the combustion zone. Due to serious concerns about ozone depletion in the stratosphere, however, the production of halons has already been prohibited along with chlorofluorocarbons (CFCs), and the development of alternative compounds is proceeding rapidly.

Recently, trifluoromethane (CHF_3, HFC−23) is suggested as one of the candidates to replace halons. Nevertheless, its inhibition mechanism is not yet known, due to the absence of kinetic data for high-temperature reactions in the fluorocarbon combustion. So, in an earlier paper,[1] we have reported the rate coefficient for the reaction $CHF_3 + H \rightarrow CF_3 + H_2$, which is an initial reaction in the CHF_3 combustion and one of the most important inhibition reactions. As the second part of our research on the flame suppression by CHF_3, we focus on the high-temperature kinetics of the subsequent reactions of CF_3 radicals with some active species in the combustion.

$$CF_3 + O(^3P) \rightarrow \text{products} \quad (1)$$

$$CF_3 + H \rightarrow \text{products} \quad (2)$$

Reactions 1 and 2 also have practical significance in the fields of plasma chemistry and atmospheric chemistry, and several kinetic studies on these reactions have been reported at room temperature. The overall rate coefficients for reactions 1 and 2 were first determined by Ryan and Plumb[2,3] using a discharge flow−mass spectroscopy technique to be $k(CF_3 + O) = (3.1\pm0.8) \times 10^{-11}$ and $k(CF_3 + H) = (8.9\pm1.8) \times 10^{-11}$ cm^3 molecule^{-1} s^{-1} at 295 K. Subsequently, Tsai and his co-workers[4,5] obtained $k(CF_3 + O) = (3.1\pm0.6) \times 10^{-11}$ and $k(CF_3 + H) = (9.1\pm1.5) \times 10^{-11}$ cm^3 molecule^{-1} s^{-1} at 293 K by the discharge-flow experiments with a photoionization mass spectrometer, in excellent accord with the results of Ryan and Plumb. On the other hand, Biordi et al.[6] reported $k(CF_3 + H) = 3.3 \times 10^{-11}$ cm^3 molecule^{-1} s^{-1} at 1540 K, which is small in comparison with the data at room temperature. This disagreement between room and high temperatures is unexpected, because the rate coefficients for atom-radical reactions generally have little temperature dependence. The data of Biordi et al. were determined in methane−oxygen−argon flames containing CF_3Br where complicated branching reactions occur simultaneously. So there is some possibility that their results are influenced by secondary reactions.

* Corresponding author. Phone: +81-3-3238-3457. Fax: +81-3-3238-3478. E-mail: takaha-k@hoffman.cc.sophia.ac.jp.

10.1021/jp9819994 CCC: $15.00
Published on Web 10/01/1998

TABLE 1: Experimental Conditions

reaction	composition of test gas mixture (ppm) CF_3I	N_2O	C_2H_5I	monitored atom	temp (K)	total density (molecules·cm^{-3})
$CF_3 + O(^3P)$	4−16	8		O and I	1900−2330	8.2×10^{18}−1.2×10^{19}
$CF_3 + H$	2.5−4		1.25−2	H and I	1150−1380	6.1×10^{18}−9.8×10^{18}

In the present research, the product channels of the $CF_3 + O(^3P)$ and $CF_3 + H$ reactions were first examined at high temperatures by calculating their branching fractions with the multichannel Rice−Ramsperger−Kassel−Marcus (RRKM) theory. Structural parameters, vibrational frequencies, and threshold energy required for the RRKM calculation were obtained from an ab initio MO calculation. Subsequently, the rate coefficients for these reactions were experimentally determined by using a shock tube−atomic resonance absorption spectroscopy technique over the temperature ranges of 1900−2330 and 1150−1380 K.

Experimental Section

Shock Tube and Optical System. All experiments were performed behind reflected shock waves in a diaphragmless stainless-steel shock tube, which consists of a 5.84-*l* driver section and a 6.2-cm i.d. and 4.6-m long test section. The details of its structure and its performance have been described previously.[1] The test section was evacuated by a turbomolecular pump to pressures down to 1×10^{-6} Torr, in which the residual gas was practically free from hydrocarbons. To measure incident shock velocity, three piezoelectric pressure transducers were mounted on the shock tube walls at 25-cm intervals from the end of the test section. Temperature and pressure of the shock-heated test gas were calculated from the incident shock velocity.

The time-resolved concentrations of electronically ground-state $O(^3P_J)$ and $H(^2S_0)$ atoms were monitored by atomic resonance absorption spectroscopy (ARAS). A microwave discharge lamp, in which helium containing a few percent of oxygen or hydrogen was flowing at a pressure of 4 Torr, was used as a light source of O- or H-ARAS. The wavelengths of monitored resonance light were 130.2, 130.4, and 130.6 nm ($^3S_1-^3P_J$) for O atoms and 121.6 nm ($^2P_{1/2}-^2S_0$) for H atoms. The resonant radiation from the lamp passed through two MgF_2 windows (1-mm thickness) mounted on the shock tube walls at a position 2 cm from the end plate. The transmitted light was isolated by a 20-cm VUV monochromator (Minutesman 302−VM), which was evacuated to a pressure less than 4×10^{-5} Torr, and detected by a solar-blind photomultiplier tube (Hamamatsu Photonics R1459). The signal was then recorded by a digital storage oscilloscope (Hitachi VC−6165).

Measurements and Gases. Measurements of the rate coefficient for the $CF_3 + O(^3P)$ reaction were carried out in mixtures of CF_3I-N_2O-Ar by detecting O atoms, while the rate coefficient for the $CF_3 + H$ was obtained from the decay of H atoms in mixtures of $CF_3I-C_2H_5I-Ar$. The details of these experimental conditions are shown in Table 1. Under the present experimental conditions, CF_3 radicals are rapidly produced through the thermal dissociation of trifluoromethyl iodide. Electronically ground-state oxygen atoms are formed through the thermal decomposition of nitrous oxide, although the production rate of O atoms is much slower than that of CF_3 radicals. Hydrogen atoms are instantaneously formed through the thermal decomposition of ethyl iodide. Oxygen and hydrogen atoms might be also generated due to wall contaminations or resident impurities, so that blank tests with argon alone were performed during the measurements, confirming the absence of background signals. For the thermal dissociation of CF_3I, equimolecular amounts of CF_3 radicals and I atoms are formed. To monitor an initial production amount of CF_3 radicals, I-ARAS ($^4P_{5/2}-^2P_{3/2}$, 183.0 nm) measurements were also carried out. The details of the calibrations for H- and I-ARAS have been described elsewhere.[1,7] The calibration experiments for O-ARAS were performed in 1−20 ppm N_2O−Ar mixtures at temperatures of approximately 2000 and 3000 K.

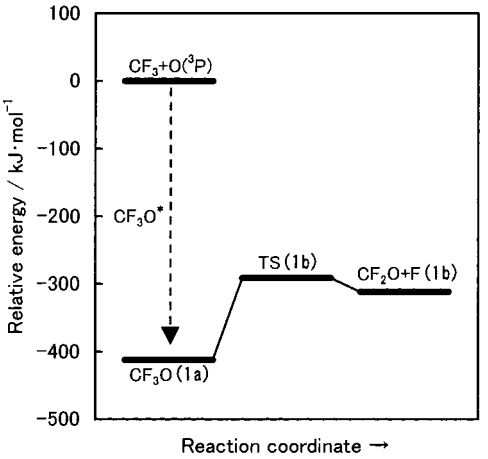

Figure 1. Energy diagram for the $CF_3 + O(^3P)$ reaction. The energies are calculated at the G2(MP2) level and are corrected for the zero-point vibrations.

High purity helium (99.995%) was used as the driver gas. Scientific grade argon (99.9999%) was used as the diluent gas. Trifluoromethyl iodide (97%) and ethyl iodide (99.0%) were purified by trap-to-trap distillation, while research grade nitrous oxide (99.99%) was used without further purification.

Results and Discussion

Theoretical Examination for Reaction Channels. To examine the product channels of the $CF_3 + O(^3P)$ and $CF_3 + H$ reactions, an ab initio MO calculation was performed by using the Gaussian 94 program.[8] Figures 1 and 2 show the energy diagrams for the $CF_3 + O(^3P)$ and $CF_3 + H$ reactions calculated at the G2(MP2) level, respectively. The $CF_3 + O(^3P)$ reaction is initiated through an electrophilic addition step of oxygen atom to trifluoromethyl radical. Since the addition step is greatly exothermic, chemically activated energized trifluoromethoxy radical, CF_3O^*, is formed. Subsequently, CF_3O^* is deactivated by the collisions with bath-gas molecules (1a) or dissociated to $CF_2O + F$ (1b). On the other hand, the first step of the $CF_3 + H$ reaction is also an electrophilic addition of H atom to trifluoromethyl radical. Vibrationally excited trifluoromethane, CHF_3^*, disappears through deactivation (2a) or F dissociation (2b) like CF_3O^*. In addition, CHF_3^* is decomposed through HF elimination (2c) occurring with the three-centered transition state. The HF elimination (2c) is superior to the F dissociation (2b) since the energy barrier for channel (2c) is much lower than that for channel (2b), as shown in Figure 2.

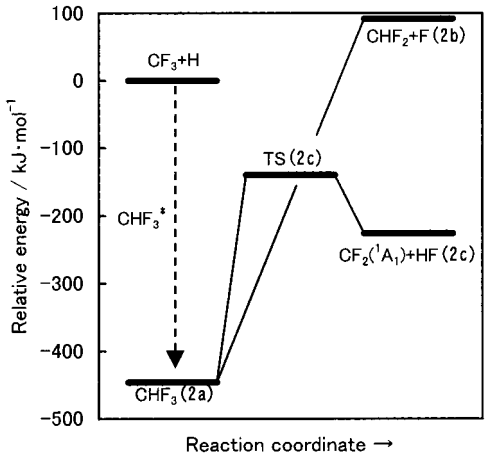

Figure 2. Energy diagram for the CF_3 + H reaction. The energies are calculated at the G2(MP2) level and are corrected for the zero-point vibrations.

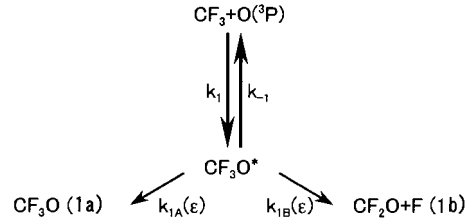

Figure 3. Model for the product channels of the CF_3 + $O(^3P)$ reaction used in the calculation of branching fractions.

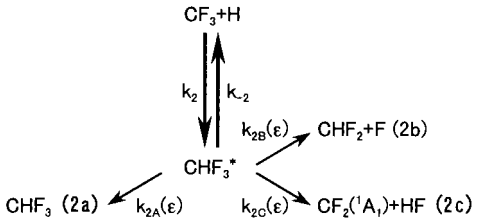

Figure 4. Model for the product channels of the CF_3 + H reaction used in the calculation of branching fractions.

The branching fraction for each product channel was calculated with the multichannel RRKM theory. For the CF_3 + $O(^3P)$ and CF_3 + H reactions, the models used in the calculation are illustrated in Figures 3 and 4. In Figure 3, the rate coefficients for channels (1a) and (1b), k_{1a} and k_{1b}, can be given as follows

$$k_{1i} = \frac{\mathrm{d[products]}/\mathrm{d}t}{[CF_3][O]} = k_1 \int_{E_{-1}}^{\infty} \frac{k_{1X}(\epsilon)}{D_1(\epsilon)} f(\epsilon)\, \mathrm{d}\epsilon$$

(i: a, b; X: A, B)

where $D_1(\epsilon) = k_{-1}(\epsilon) + k_{1A}(\epsilon) + k_{1B}(\epsilon)$ and E_{-1} is threshold energy for reaction −1. The chemical activation distribution function at a specific energy ϵ, $f(\epsilon)$, can be expressed as

$$f(\epsilon) = \frac{g(\epsilon)\exp(-\epsilon/k_B T)}{\int_0^{\infty} g(\epsilon)\exp(-\epsilon/k_B T)\,\mathrm{d}\epsilon}$$

where $g(\epsilon)$ is the density of states and k_B is the Boltzmann constant. The RRKM rate coefficients were applied for $k_{-1}(\epsilon)$ and $k_{1B}(\epsilon)$

$$k_{RRKM}(\epsilon) = \frac{Q_r^{\ddagger}}{Q_r} \frac{G(\epsilon - E_0)}{hg(\epsilon)}$$

TABLE 2: RRKM Parameters for the CF_3 + $O(^3P)$ Reaction

	$CF_3O^* \rightarrow CF_3O^{\ddagger}$			
		transition state		
	reactant	TS(−1)[a]		
	CF_3O	model I	model II	TS(1b)
E_0 (kJ·mol^{-1})		412.2[b]		120.8
reaction path degeneracy		1		3
moments of inertia				
I_a (10^{-38} g·cm^2)	1.403	1.479[c]	1.511[d]	1.282
I_b (10^{-38} g·cm^2)	1.448	1.683[c]	3.385[d]	1.596
I_c (10^{-38} g·cm^2)	1.516	1.689[c]	3.385[d]	1.747
vibrational frequencies (cm^{-1})	1310	1286[e]		1483
	1278	1286[e]		1333
	1275	1086[e]		919
	883	677[e]		578
	607	491[e]		559
	583	491[e]		446
	572	409[f]	110[f]	304
	411	393[f]	110[f]	250
	223			

[a] Channel without a saddle point. See the text for models I and II. [b] Calculated dissociation energy of the bond being broken at 0 K. [c,d] Calculated from the geometries optimized partially at r(C−O) = 1.776 and 3.142 Å. [e] Frequencies calculated for CF_3. [f] Soft bending frequency of the bond being broken, estimated from that for CF_3O (see the text).

where E_0 is threshold energy for each channel, $G(\epsilon - E_0)$ is the sum of states, and h is the Planck constant. Q_r and $Q_r^{\ddagger}$ are the rotational partition functions for the energized reactant and the transition state, respectively. The density of states and the sum of states were calculated by using the Whitten−Rabinovitch formulas.[9,10] On the other hand, the deactivation rate coefficient $k_{1A}(\epsilon)$ was given as the product of the Lennard−Jones (L−J) collision frequency Z_{LJ} and the collision efficiency β_c. The β_c value was evaluated from Troe's expression.[11] The average energy transferred per collision for bath-gas argon $-\langle\Delta E\rangle$, which was necessary to calculate β_c, was taken to be 310 cm^{-1} from Gardiner and Troe.[12]

For the CF_3 + H system, the rate coefficients for channels (2a) to (2c), k_{2a} to k_{2c}, can also be given as follows

$$k_{2i} = \frac{\mathrm{d[products]}/\mathrm{d}t}{[CF_3][H]} = k_2 \int_{E_{-2}}^{\infty} \frac{k_{2X}(\epsilon)}{D_2(\epsilon)} f(\epsilon)\, \mathrm{d}\epsilon$$

(i: a, b, c; X: A, B, C)

where $D_2(\epsilon) = k_{-2}(\epsilon) + k_{2A}(\epsilon) + k_{2B}(\epsilon) + k_{2C}$ and E_{-2} is threshold energy for reaction −2. The RRKM rate coefficients were applied for $k_{-2}(\epsilon)$, $k_{2B}(\epsilon)$, and $k_{2C}(\epsilon)$, while the values of $Z_{LJ}\beta_c$ were substituted for $k_{2A}(\epsilon)$.

The L−J parameters are required to calculate the deactivation rate coefficients $k_{1A}(\epsilon)$ and $k_{2A}(\epsilon)$. The parameters σ_{LJ} and ϵ_{LJ}/k_B were taken from the NASA technical report[13] to be 4.33 Å and 240 K for CHF_3 and to be 3.542 Å and 93.3 K for Ar. Since the L−J parameters for CF_3O were unknown, they were estimated from the polarizability as described by Cambi et al.[14] The polarizability of CF_3O was derived by the ab initio MO calculation at the HF/6−31G(d) level. Thus, the parameters σ_{LJ} and ϵ_{LJ}/k_B were found to be 3.90 Å and 262 K for CF_3O. The RRKM parameters for the CF_3 + $O(^3P)$ and CF_3 + H reactions are summarized in Tables 2 and 3, respectively. The geometries of the reactants and the transition states for the channels with a saddle point were optimized by an ab initio MO calculation at MP2(full)/6−31G(d) level, and their threshold energies E_0's were calculated at the G2(MP2) level. The

TABLE 3: RRKM Parameters for the CF_3 + H Reaction

	$CHF_3^* \rightarrow CHF_3^{\ddagger}$					
		transition state				
		TS(−2)[a]		TS(2b)[a]		
	reactant CHF_3	model I	model II	model I	model II	TS(2c)
E_0 (kJ·mol^{-1})		446.2[b]		539.3[b]		306.6
reaction path degeneracy		1		3		3
moments of inertia						
I_a (10^{-38} g·cm^2)	0.8213	0.8324[c]	0.9109[d]	0.8214[e]	0.8605[f]	0.7674
I_b (10^{-38} g·cm^2)	0.8213	0.8324[c]	0.9114[d]	1.097[e]	2.760[f]	1.258
I_c (10^{-38} g·cm^2)	1.498	1.493[c]	1.507[d]	1.758[e]	3.429[f]	1.900
vibrational frequencies (cm^{-1})	3036	1286[g]		3305[h]		2300
	1414	1286[g]		1343[h]		1363
	1414	1086[g]		1181[h]		1226
	1186	677[g]		1150[h]		1188
	1186	491[g]		1041[h]		831
	1127	491[g]		521[h]		627
	681	1033[i]	362[i]	334[i]	92[i]	250
	492	1033[i]	362[i]	334[i]	92[i]	206
	492					

[a] Channel without a saddle point. See the text models I and II. [b] Calculated dissociation energy of the bond being broken at 0 K. [c,d] Calculated from the geometries optimized partially at r(C−H) = 1.415 and 2.504 Å. [e,f] Calculated from the geometries optimized partially at r(C−F) = 1.746 and 3.089 Å. [g,h] Frequencies calculated for CF_3 and CHF_2. [i] Soft bending frequency of the bond being broken, estimated from that for CHF_3 (see the text).

vibrational frequencies were computed at the HF/6−31G(*d*) level and scaled by a factor of 0.8929[15] to eliminate known systematic errors. As channels (−1), (−2), and (2b) were the dissociation channels without a saddle point, two models were adopted as the critical configurations for these channels. The geometries of TS(−1), (−2), and (2b) were determined by the MP2(full)/6−31G(*d*) partial optimization, during which the lengths of the bonds being broken were fixed to 1.3 times (model I) and 2.3 times (model II) the lengths at their equilibrium structures, because the looseness of the critical configurations for simple-bond-fission channels was generally within this range. For these channels, the bond dissociation energies calculated at the G2(MP2) level were substituted for the threshold energies E_0's. In the vibrational motion for these critical configurations, the frequencies representing the soft bending vibrations of the bonds being broken were evaluated from the following formula[16]

$$\nu(r) = \nu(r_e) \exp\left(-\frac{r - r_e}{1.04\ \text{Å}}\right)$$

where r is the length of the bond being broken (= $1.3r_e$ and $2.3r_e$ for models I and II, respectively) and r_e is its equilibrium length. The remaining vibrational frequencies were taken from the frequencies calculated for the products. Such approximation of the RRKM parameters for $k_{-1}(\epsilon)$, $k_{-2}(\epsilon)$, and $k_{2B}(\epsilon)$ is rather rough; but it is acceptable, because these channels have higher energy barriers and so they are inferior to other competing channels.

Table 4 shows the branching fraction calculated for each product channel of the CF_3 + $O(^3P)$ and CF_3 + H reactions at high temperatures. The results completely agreed between models I and II in this calculation. The branching fractions of the F dissociation channel (1b) for the CF_3 + $O(^3P)$ reaction and the HF elimination channel (2c) for the CF_3 + H reaction are more than 99%; the other channels are negligible for both the reactions. The pressures at which the branching fractions of the deactivation channels (1a) and (2a) are more than 1% over the temperature range of 1200−2000 K were calculated to be 310−780 and 10−30 atm for the CF_3 + $O(^3P)$ and CF_3 + H reactions, respectively, and so these deactivation processes contribute only at rather high pressures.

TABLE 4: Branching Fractions Calculated for the CF_3 + $O(^3P)$ and CF_3 + H Reactions

			branching fraction[a] (%)			
			1200 K		2000 K	
reaction channel			model I	model II	model I	model II
$CF_3 + O(^3P) \rightarrow$	CF_3O	(1a)	0.005	0.005	0.004	0.004
	$CF_2O + F$	(1b)	99.995	99.995	99.996	99.996
$CF_3 + H \rightarrow$	CHF_3	(2a)	0.158	0.158	0.092	0.092
	$CHF_2 + F$	(2b)	0.000	0.000	0.000	0.000
	$CF_2(^1A_1) + HF$	(2c)	99.842	99.842	99.908	99.908

[a] Calculated at [M] = 1×10^{19} molecules·cm^{-3}.

The reliability of these theoretical predictions greatly depends on the accuracy of the threshold energy E_0, because E_0 is the most sensitive parameter in the calculation. In the present calculation, the G2(MP2) energies were used as E_0's. For the CF_3 + H reaction, if E_0 of TS(−2) is overestimated or if E_0 of TS(2c) is underestimated, the calculation must yield a small branching fraction to the deactivation channels (2a). In practice, when E_0 of TS(−2) is decreased by 70 kJ·mol^{-1} or when E_0 of TS(2c) is increased by 40 kJ·mol^{-1}, the branching fraction of channel (2a) becomes more than 1% at 1250 K. For the CF_3 + $O(^3P)$ reaction, the revision of E_0 by more than 100 kJ·mol^{-1} gives the branching fraction of 1% to channel (1a). However, such a great error cannot be included in E_0, because the average absolute deviation was reported to be ±6.61 kJ·mol^{-1} for various relative energies calculated at the G2(MP2) level.[17] Therefore, we can conclude that the productions of CF_2O + F and $CF_2(^1A_1)$ + HF are the only channels possible under the present conditions for the CF_3 + $O(^3P)$ and CF_3 + H reactions, respectively.

Determination of Rate Coefficients. Preliminarily, the calibration experiments for O-ARAS were performed in mixtures of N_2O highly diluted in argon. Figure 5 shows the calibration curves which were prepared by making the O-atom absorbance at the steady-state correspond to the initial concentration of N_2O. The Lambert−Beer law cannot be applied in the present study. The apparent absorption coefficients, which mean the tangential slopes of the calibration curves, decrease with the O-atom concentration due to self-absorption or self-

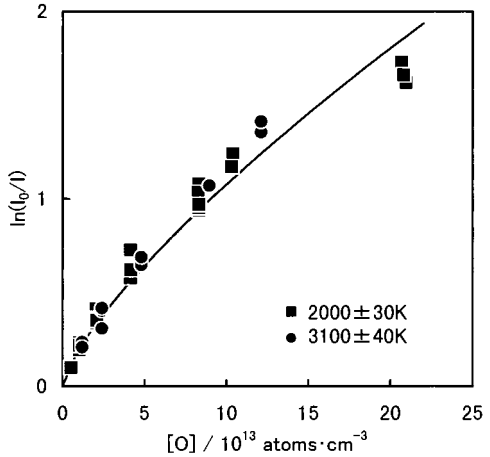

Figure 5. Calibration curves for O-ARAS at $T = (\blacksquare)$ 2000 ± 30 and $(\bullet)$ 3100 ± 40 K. The solid line denotes the curves fitted by the least-squares method (see text).

reversal. The temperature dependence was not found. Assuming the modified Lambert−Beer equation, we determined two parameters of α and γ by a least-squares method as follows:

$$\ln \frac{I_0}{I} = \alpha[\mathrm{O}]^{\gamma}$$

$$\alpha = 10^{-10.40\pm0.24}\ \mathrm{cm}^{2.25}\ \mathrm{atom}^{-0.75}$$

$$\gamma = 0.746 \pm 0.018$$

The calibration curve calculated from this expression approximates the experimental data well, as shown in Figure 5. This result indicates that an absorption of 50% corresponds to a concentration of 5.3×10^{13} atoms·cm^{-3}, which is consistent with the value reported by Klatt et al.,[18] but larger than that in Thielen and Roth's data (1.5×10^{13} atoms·cm^{-3}).[19] The sensitivity for O-ARAS depends on the light path length for absorption and additionally on the experimental conditions under which the light source are operated. Thielen and Roth performed the experiments in a 7.9-cm i.d. shock tube and used 1% O_2−He mixture as a light source of O-ARAS to prevent the self-absorption. Due to longer light path and less self-absorption, they established a more sensitive O-atom detection system than we have done. Taking account of these factors, we can conclude that the sensitivity for O-ARAS measured in the present work is reasonable in comparison with the results previously reported by many workers.[20]

Measurements of the rate coefficient for the reaction 1b were performed in mixtures of CF_3I and N_2O highly diluted in argon.

$$CF_3 + O(^3P) \rightarrow CF_2O + F \qquad (1b)$$

Figure 6 shows typical concentration profiles of O atoms in 8 ppm N_2O−Ar mixtures (a) without CF_3I and (b) with 8 ppm CF_3I. These absolute concentrations were converted using the above approximate formula from the absorption at 130.2−130.6 nm. In the N_2O−Ar mixture, the O-atom concentration increases gradually through reaction 31 to reach a saturated value, while in the presence of CF_3I, oxygen atoms get to a maximum value at 200 μs and then decay.

$$N_2O + M \rightarrow N_2 + O + M \qquad (31)$$

Figure 6c shows the concentration profile of I atoms measured under the same conditions as Figure 6b. Due to thermal

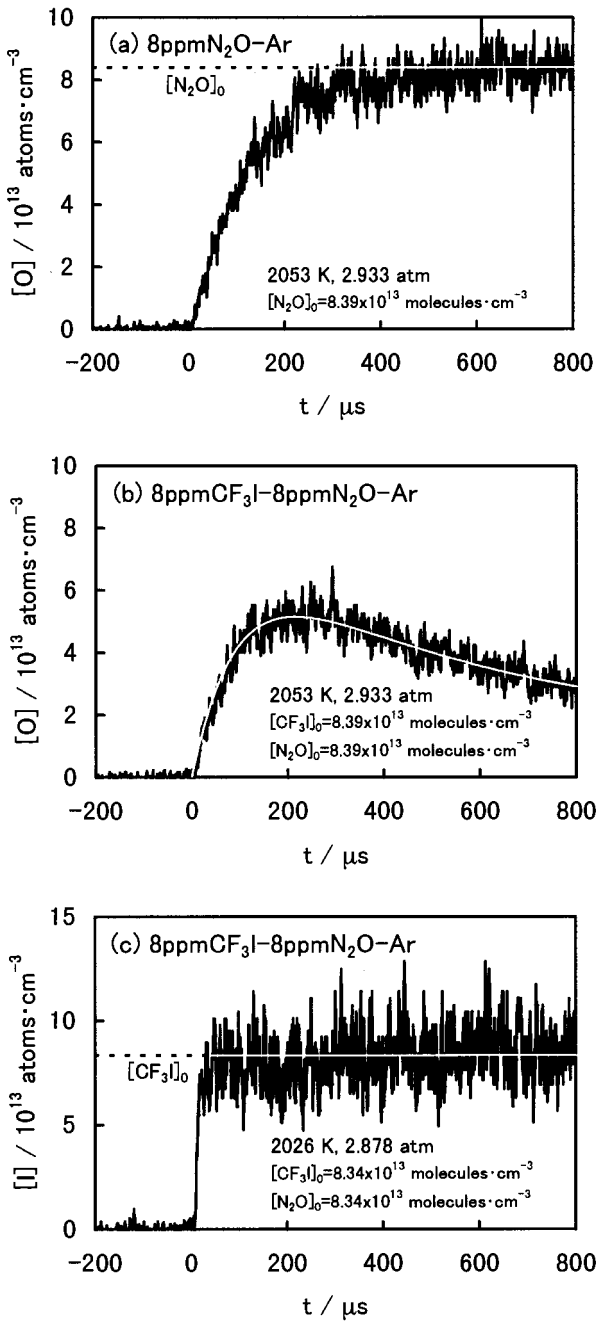

Figure 6. Typical concentration profiles of (a) O atoms in 8 ppm N_2O−Ar, (b) O atoms in 8 ppm CF_3I−8 ppm N_2O−Ar, and (c) I atoms in 8 ppm CF_3I−8 ppm N_2O−Ar mixtures. The white curve in part (b) denotes the profile calculated in the reaction scheme of Table 5.

dissociation of CF_3I, the I-atom concentration immediately jumps to an equivalent value with the initial CF_3I concentration.

$$CF_3I(+M) \rightarrow CF_3 + I(+M) \qquad (11)$$

The comparison between Figure 6b,c indicates that the production of CF_3 radicals via reaction 11 completes before the O-atom production. From the kinetic data for reaction 11,[21] the times when 99% of CF_3I is dissociated to CF_3 + I are estimated to be 1.38 μs at 1900 K and 0.33 μs at 2330 K with a total density of 1.0×10^{19} molecules·cm^{-3}. These experimental and calculated results confirm that the O-atom decay after 200 μs found in Figure 6b is caused by the $CF_3 + O(^3P)$ reaction but not by the $CF_3I + O(^3P)$ reaction.

On the other hand, the rate coefficient for reaction 2c was measured in mixtures of CF_3I and C_2H_5I highly diluted in argon.

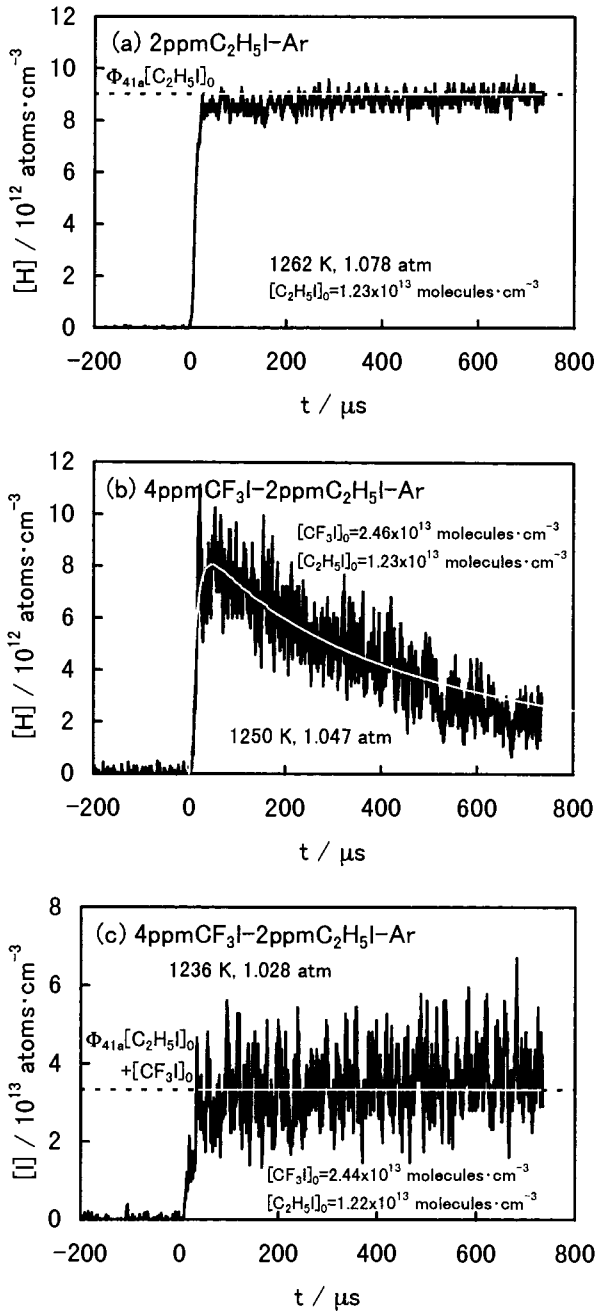

Figure 7. Typical concentration profiles of (a) H atoms in 2 ppm C_2H_5I-Ar, (b) H atoms in 4 ppm CF_3I-2 ppm C_2H_5I-Ar, and (c) I atoms in 4 ppm CF_3I-2 ppm C_2H_5I-Ar mixtures. In parts (a) and (c), Φ_{41a} means the branching ratio, $k_{41a}/(k_{41a} + k_{41b})$, of the thermal decomposition reactions 41a and 41b of C_2H_5I shown in Table 6. The white curve in part (b) denotes the profile calculated in the reaction scheme of Table 6.

$$CF_3 + H \rightarrow CF_2(^1A_1) + HF \qquad (2c)$$

Figure 7 shows typical concentration profiles of H atoms in 2 ppm C_2H_5I-Ar mixtures (a) without CF_3I and (b) with 4 ppm CF_3I. In the C_2H_5I-Ar mixture, the H-atom concentration rapidly raises to reach a nearly constant value. At temperatures above 1100 K, ethyl iodide is decomposed via the following two channels.

$$C_2H_5I \rightarrow C_2H_5 + I \qquad (41a)$$

$$C_2H_5I \rightarrow C_2H_4 + HI \qquad (41b)$$

TABLE 5: Reaction Scheme for the CF_3I-N_2O System

			forward rate coefficient[a]			
no.	reaction		log *A*	*n*	E_a/R	ref
1b	$CF_3 + O = CF_2O + F$		adjusted			
11	$CF_3I(+M) = CF_3 + I(+M)$	high	14.40	0.00	26500	21
		low	−9.15	0.00	14500	21
12	$CF_3I + I = CF_3 + I_2$		−10.47	0.00	8540	22
14	$CF_3 + CF_3 = C_2F_6$		−10.50	0.00	0	23
21	$F + F + M = F_2 + M$		−33.56	0.00	0	24
25	$I + I + M = I_2 + M$		−34.57	−1.00	0	24
31	$N_2O + M = N_2 + O + M$		0.06	−2.50	32710	25
32	$O + O + M = O_2 + M$		−34.28	0.00	−900	26

[a] Forward rate coefficients in the form $k = AT^n \exp(-E_a/RT)$, in cm^3, molecule, and s units. Reverse rate coefficients were calculated from the forward ones and the equilibrium constants.

TABLE 6: Reaction Scheme for the $CF_3I-C_2H_5I$ System

			forward rate coefficient[a]			
no.	reaction		log *A*	*n*	E_a/R	ref
2c	$CF_3 + H = CF_2(^1A_1) + HF$		adjusted			
11	$CF_3I(+M) = CF_3 + I(+M)$	high	14.40	0.00	26500	21
		low	−9.15	0.00	14500	21
12	$CF_3I + I = CF_3 + I_2$		−10.47	0.00	8540	22
13	$CF_3I + H = CF_3 + HI$		−10.08	0.00	510	27
14	$CF_3 + CF_3 = C_2F_6$		−10.50	0.00	0	23
15	$CF_2(^1A_1) + H = CF + HF$		−10.40	0.00	0	5
21	$F + F + M = F_2 + M$		−33.56	0.00	0	24
22	$F_2 + H = HF + F$		−9.70	0.00	1210	24
23	$F + H + M = HF + M$		−29.58	−1.00	0	24
24	$HF + H = H_2 + F$		−9.44	0.00	17000	24
25	$I + I + M = I_2 + M$		−34.57	−1.00	0	24
26	$I_2 + H = HI + I$		−9.39	0.00	0	24
27	$I + H + M = HI + M$		−34.48	−1.00	0	24
28	$HI + H = H_2 + I$		−10.26	0.00	0	24
41a	$C_2H_5I = C_2H_5 + I$		11.79	0.00	20200	28
41b	$C_2H_5I = C_2H_4 + HI$		11.11	0.00	19500	28
42	$C_2H_5I + I = C_2H_5 + I_2$		−10.18	0.00	8410	24
43	$C_2H_5I + H = C_2H_5 + HI$		−9.24	0.00	1760	24
44	$C_2H_4 + H(+M) = C_2H_5(+M)$	high	−10.44	0.00	1030	29
		low	−19.76	−2.80	−24	29
45	$H + H + M = H_2 + M$		−29.56	−1.00	0	29

[a] Forward rate coefficients in the form $k = AT^n \exp(-E_a/RT)$, in cm^3, molecule, and s units. Reverse rate coefficients were calculated from the forward ones and the equilibrium constants.

The ethyl radicals produced through reaction 41a immediately decay to become ethylene and hydrogen atoms.

$$C_2H_5(+M) \rightarrow C_2H_4 + H(+M) \qquad (-44)$$

If other reactions producing and consuming hydrogen atoms do not occur along with the above reactions, the final H-atom concentration $[H]_f$ can be related to the initial concentration of ethyl iodide by the following formula

$$[H]_f = \Phi_{41a}[C_2H_5I]_0$$

where Φ_{41a} is the branching ratio, $k_{41a}/(k_{41a} + k_{41b})$. As shown in Figure 7a, $[H]_f$ calculated from this expression is in good agreement with the final value of H-atom concentration obtained experimentally. This confirms that the formation of hydrogen atom from ethyl iodide can be explained only by reactions 41a, 41b, and −44.

As shown in Figure 7b, the addition of CF_3I apparently reduces H atoms as well as O atoms. Figure 7c shows the concentration profile of I atoms measured under the same conditions as Figure 7b. The I-atom concentration rapidly jumps to an equivalent value with the sum of $[CF_3I]_0$ and $\Phi_{41a}[C_2H_5I]_0$.

TABLE 7: Summary of Rate Coefficients Measured for the Reaction $CF_3 + O(^3P) \rightarrow CF_2O + F$ (1b)

		reflected shock region				
P_1[a] (Torr)	U_s[b] (m·ms^{-1})	T (K)	[M] (molecules·cm^{-3})	$[CF_3I]_0$ (molecules·cm^{-3})	$[N_2O]_0$ (molecules·cm^{-3})	k_{1b} (cm^3 molecule^{-1} s^{-1})
			[M] = (8.24 ± 0.09) × 10^{18} molecules·cm^{-3}			
41.0	0.906	1912	8.34 × 10^{18}	6.67 × 10^{13}	6.67 × 10^{13}	2.16 × 10^{-11}
40.0	0.920	1969	8.24 × 10^{18}	6.59 × 10^{13}	6.59 × 10^{13}	2.33 × 10^{-11}
40.0	0.929	2006	8.30 × 10^{18}	6.64 × 10^{13}	6.64 × 10^{13}	2.33 × 10^{-11}
40.0	0.931	2015	8.32 × 10^{18}	6.66 × 10^{13}	6.66 × 10^{13}	2.33 × 10^{-11}
40.0	0.938	2043	8.37 × 10^{18}	6.70 × 10^{13}	6.70 × 10^{13}	2.33 × 10^{-11}
40.0	0.939	2046	8.38 × 10^{18}	6.70 × 10^{13}	6.70 × 10^{13}	2.49 × 10^{-11}
39.0	0.946	2074	8.21 × 10^{18}	6.57 × 10^{13}	6.57 × 10^{13}	2.82 × 10^{-11}
39.0	0.954	2106	8.26 × 10^{18}	6.61 × 10^{13}	6.61 × 10^{13}	2.99 × 10^{-11}
38.0	0.954	2109	8.06 × 10^{18}	6.45 × 10^{13}	6.45 × 10^{13}	2.82 × 10^{-11}
38.0	0.970	2174	8.15 × 10^{18}	6.52 × 10^{13}	6.52 × 10^{13}	2.82 × 10^{-11}
38.0	0.974	2193	8.18 × 10^{18}	6.55 × 10^{13}	6.55 × 10^{13}	2.33 × 10^{-11}
38.0	0.976	2200	8.19 × 10^{18}	6.55 × 10^{13}	6.55 × 10^{13}	2.66 × 10^{-11}
38.0	0.985	2239	8.25 × 10^{18}	6.60 × 10^{13}	6.60 × 10^{13}	2.49 × 10^{-11}
38.0	0.999	2398	8.33 × 10^{18}	6.66 × 10^{13}	6.66 × 10^{13}	2.49 × 10^{-11}
37.0	1.004	2321	8.14 × 10^{18}	6.51 × 10^{13}	6.51 × 10^{13}	2.49 × 10^{-11}
37.0	1.004	2323	8.14 × 10^{18}	6.51 × 10^{13}	6.51 × 10^{13}	2.49 × 10^{-11}
			[M] = (1.24 ± 0.01) × 10^{19} molecules·cm^{-3}			
61.0	0.904	1906	1.24 × 10^{19}	9.91 × 10^{13}	9.91 × 10^{13}	2.49 × 10^{-11}
61.0	0.906	1914	1.24 × 10^{19}	9.93 × 10^{13}	9.93 × 10^{13}	2.49 × 10^{-11}
61.0	0.909	1925	1.24 × 10^{19}	9.95 × 10^{13}	9.95 × 10^{13}	2.33 × 10^{-11}
60.0	0.927	1999	1.24 × 10^{19}	9.95 × 10^{13}	9.95 × 10^{13}	2.49 × 10^{-11}
60.0	0.930	2011	1.25 × 10^{19}	9.98 × 10^{13}	9.98 × 10^{13}	2.82 × 10^{-11}
60.0	0.933	2020	1.25 × 10^{19}	1.00 × 10^{14}	1.00 × 10^{14}	2.66 × 10^{-11}
58.0	0.944	2068	1.22 × 10^{19}	9.76 × 10^{13}	9.76 × 10^{13}	2.33 × 10^{-11}
58.0	0.949	2087	1.22 × 10^{19}	9.79 × 10^{13}	9.79 × 10^{13}	2.99 × 10^{-11}
58.0	0.953	2103	1.23 × 10^{19}	9.82 × 10^{13}	9.82 × 10^{13}	2.82 × 10^{-11}

[a] Pressure ahead of incident shock wave. [b] Incident shock velocity.

TABLE 8: Summary of Rate Coefficients Measured for the Reaction $CF_3 + H \rightarrow CF_2(^1A_1) + HF$ (2c)

		reflected shock region				
P_1[a] (Torr)	U_s[b] (m·ms^{-1})	T (K)	[M] (molecules·cm^{-3})	$[CF_3I]_0$ (molecules·cm^{-3})	$[C_2H_5I]_0$ (molecules·cm^{-3})	k_{2c} (cm^3 molecule^{-1} s^{-1})
			[M] = (6.13 ± 0.05) × 10^{18} molecules·cm^{-3}			
40.0	0.688	1157	6.14 × 10^{18}	2.46 × 10^{13}	1.23 × 10^{13}	9.13 × 10^{-11}
40.0	0.696	1180	6.23 × 10^{18}	2.49 × 10^{13}	1.25 × 10^{13}	8.97 × 10^{-11}
39.0	0.696	1182	6.08 × 10^{18}	2.43 × 10^{13}	1.22 × 10^{13}	9.05 × 10^{-11}
39.0	0.706	1211	6.18 × 10^{18}	2.47 × 10^{13}	1.24 × 10^{13}	8.88 × 10^{-11}
38.0	0.712	1229	6.08 × 10^{18}	2.43 × 10^{13}	1.22 × 10^{13}	8.88 × 10^{-11}
38.0	0.715	1239	6.11 × 10^{18}	2.44 × 10^{13}	1.22 × 10^{13}	8.65 × 10^{-11}
38.0	0.718	1250	6.15 × 10^{18}	2.46 × 10^{13}	1.23 × 10^{13}	9.13 × 10^{-11}
38.0	0.719	1251	6.15 × 10^{18}	2.46 × 10^{13}	1.23 × 10^{13}	9.22 × 10^{-11}
37.0	0.728	1279	6.08 × 10^{18}	2.43 × 10^{13}	1.22 × 10^{13}	8.64 × 10^{-11}
37.0	0.737	1309	6.16 × 10^{18}	2.46 × 10^{13}	1.23 × 10^{13}	9.13 × 10^{-11}
37.0	0.741	1323	6.20 × 10^{18}	2.48 × 10^{13}	1.24 × 10^{13}	8.72 × 10^{-11}
36.0	0.746	1338	6.08 × 10^{18}	2.43 × 10^{13}	1.22 × 10^{13}	8.85 × 10^{-11}
36.0	0.748	1344	6.09 × 10^{18}	2.44 × 10^{13}	1.22 × 10^{13}	9.55 × 10^{-11}
36.0	0.751	1353	6.12 × 10^{18}	2.45 × 10^{13}	1.22 × 10^{13}	8.97 × 10^{-11}
			[M] = (9.81 ± 0.04) × 10^{18} molecules·cm^{-3}			
64.0	0.687	1154	9.82 × 10^{18}	2.45 × 10^{13}	1.23 × 10^{13}	8.30 × 10^{-11}
63.0	0.694	1176	9.79 × 10^{18}	2.45 × 10^{13}	1.22 × 10^{13}	8.47 × 10^{-11}
62.0	0.703	1203	9.78 × 10^{18}	2.44 × 10^{13}	1.22 × 10^{13}	8.88 × 10^{-11}
61.0	0.715	1240	9.82 × 10^{18}	2.45 × 10^{13}	1.23 × 10^{13}	9.13 × 10^{-11}
60.0	0.725	1271	9.81 × 10^{18}	2.45 × 10^{13}	1.23 × 10^{13}	8.64 × 10^{-11}
59.0	0.734	1299	9.78 × 10^{18}	2.44 × 10^{13}	1.22 × 10^{13}	8.47 × 10^{-11}
58.0	0.751	1356	9.87 × 10^{18}	2.47 × 10^{13}	1.23 × 10^{13}	8.30 × 10^{-11}
58.0	0.752	1359	9.88 × 10^{18}	2.47 × 10^{13}	1.24 × 10^{13}	9.13 × 10^{-11}
57.0	0.757	1373	9.77 × 10^{18}	2.44 × 10^{13}	1.22 × 10^{13}	8.64 × 10^{-11}

[a] Pressure ahead of incident shock wave. [b] Incident shock velocity.

This result confirms that the thermal dissociation of CF_3I (11) immediately completes even over the relative low temperature ranges of 1100−1380 K and that the H-atom decay found in Figure 7b is caused by the $CF_3 + H$ reaction.

To determine the rate coefficients for reactions 1b and 2c, k_{1b} and k_{2c}, the concentration profiles of O and H atoms were calculated by numerically integrating the rate equations in the appropriate reaction schemes of Tables 5 and 6. The values of k_{1b} and k_{2c} were adjusted so that the calculated curves most closely matched the observed ones, as shown in Figures 6b and 7b. Rate coefficient data for reactions 1b and 2c, derived under various experimental conditions, are summarized in Tables 7 and 8, and the Arrhenius plots of k_{1b} and k_{2c} are shown in Figures 8 and 9, respectively. Neither rate coefficient had and

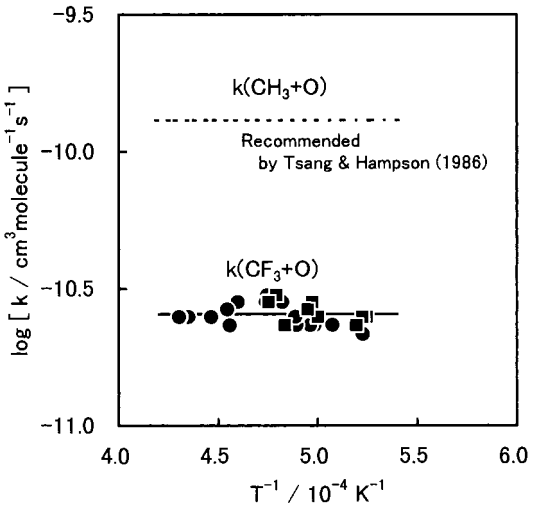

Figure 8. Arrhenius plot of the rate coefficients for the $CF_3 + O(^3P)$ reaction. (●) and (■) denote the present results measured at [M] = 8.2×10^{18} and 1.2×10^{19} molecules·cm^{-3}, respectively. (− − −) The rate coefficient for the $CH_3 + O$ reaction recommended by Tsang and Hampson.[36]

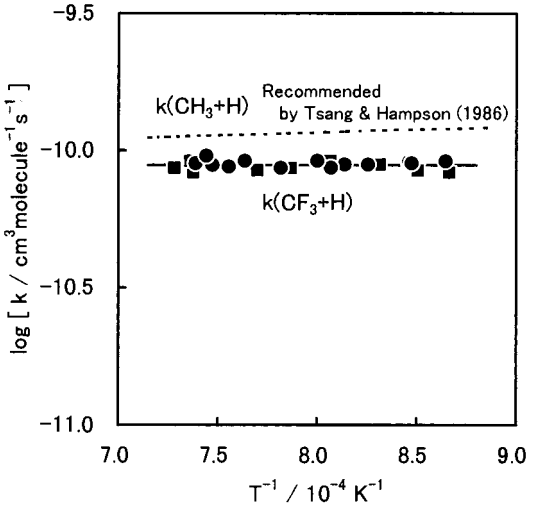

Figure 9. Arrhenius plot of the rate coefficients for the $CF_3 + H$ reaction. (●) and (■) denote the present results measured at [M] = 6.1×10^{18} and 9.8×10^{18} molecules·cm^{-3}, respectively. (− − −) The rate coefficient for the $CH_3 + H$ reaction recommended by Tsang and Hampson.[36]

temperature or pressure dependence; the values were determined to be $k_{1b} = (2.55 \pm 0.23) \times 10^{-11}$ and $k_{2c} = (8.86 \pm 0.32) \times 10^{-11}$ cm^3 molecule^{-1} s^{-1} over the temperature ranges of 1900−2330 and 1150−1380 K (error limits at the one standard deviation level). These results were in good agreement with some room-temperature data reported by Ryan and Plumb[2,3] and Tsai and his co-workers.[4,5] This agreement looks reasonable, because the rate coefficients for atom-radical reactions generally have little temperature dependence. At high temperatures, k_{2c} were researched by Biordi et al.,[6] but k_{1b} was not yet studied. The previous k_{2c} data of Biordi et al. is only one-third of the value yielded in this work. Their data were determined by monitoring CF_2 radicals in methane−oxygen−argon flames containing CF_3-Br, where complicated branching reactions occur simultaneously. Furthemore, an initial concentration of CF_3Br which Biordi et al. have used as a precursor of CF_3 radical is three powers of ten higher than our initial concentration of the precursor (CF_3I). So there is some possibility that their results are influenced by other secondary reactions.

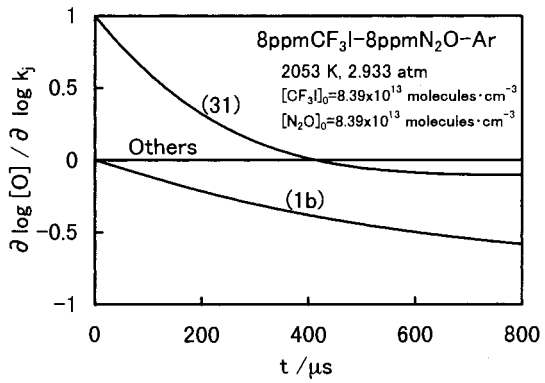

Figure 10. Sensivity analysis of the rate coefficients for O-atom concentration in 8 ppm CF_3I−8 ppm N_2O−Ar mixture. Numbers in the figure denote the reaction numbers given in Table 5.

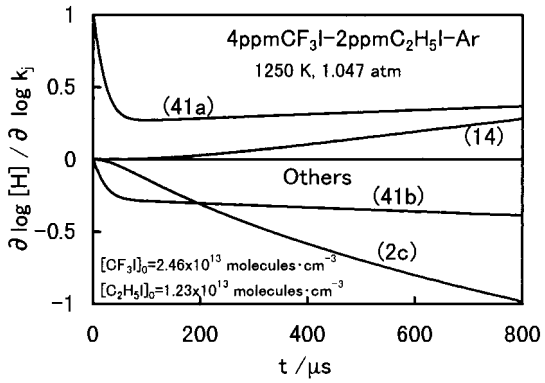

Figure 11. Sensivity analysis of the rate coefficients for H-atom concentration in 4 ppm CF_3I−2 ppm C_2H_5I−Ar mixture. Numbers in the figure denote the reaction numbers given in Table 6.

In this study, the rate coefficients for reactions 1b and 2c were determined indirectly by fitting the O- and H-atom concentration profiles calculated by using the reaction schemes proposed in Tables 5 and 6 to the observed ones. To check the influence of secondary reactions on the determination of k_{1b} and k_{2c}, sensitivity analyses were made by using the CHEMKIN−II[30] and SENKIN[31] program codes. In the CF_3I-N_2O−Ar and $CF_3I-C_2H_5I$−Ar mixtures, typical time-resolved profiles of the normalized first-order sensitivity coefficients for O- and H-atom concentrations, $\partial(\log[O])/(\partial \log k_j)$ and $\partial(\log[H])/(\partial \log k_j)$, are shown in Figures 10 and 11, respectively. In the CF_3I-N_2O−Ar mixture, the calculation shows that other side reactions besides reactions 1b and 31 have no influence on O-atom concentration. Reaction 31 is the most sensitive until 200 μs, when O-atom concentration gets to a maximum (cf. Figure 6b), but the focus reaction 1b strongly affects the O-atom concentration instead of reaction 31 after 200 μs. The kinetic data for reaction 31 have already been reported by numerous workers. Some extensive literature reviews[25,32] about it have also been published. In this work, k_{31} is cited from the review of Hanson and Salimian,[25] and it is examined to have only an error of ±20% in the review. If k_{31} have a large error, the calculated O-atom concentration profiles cannot be fitted to the observed ones by adjusting k_{1b} only, because reaction 31 has more sensitivity at the early stage of reaction time but reaction 1b contributes later. Therefore, the uncertainty of k_{31} cannot be considered to influence the determination of k_{1b} directly. In the $CF_3I-C_2H_5I$−Ar mixture, reactions 2c, 41a, and 41b have relatively high sensitivity to H-atom concentration. In contrast, reactions 11−13, 15, 21−28, and 42−45 give no effect. Since the kinetic data for reactions 41a and 41b cited in this work

have directly and exactly been measured by using a shock tube−ARAS technique by our group,[28] these rate coefficients cannot create a large error in the determination of k_{2c}. The sensitivity coefficient for reaction 14 is also not 0 but is very small. For example, an uncertainty of ±50% for k_{14} only causes an error of 3−5% to k_{2c}. Therefore, we can conclude that k_{2c} has little serious error due to the uncertainty of kinetic data for these side reactions.

The rate coefficients of collisions between CF_3 and $O(^3P)$ and between CF_3 and H were calculated with electronic degeneracy factors g's under the L−J interaction potentials.[33]

$$k_{LJ} = \left(\frac{g^{\ddagger}}{g_1 g_2}\right)\sigma_{12}^2\,\Omega_{12}^{(2,2)*}\left(\frac{8\pi k_B T}{\mu_{12}}\right)^{1/2}$$

where μ_{12} is the reduced mass between CF_3 radical and O or H atom. The reduced collision integral $\Omega_{12}^{(2,2)*}$ was given by Troe's approximation.[11] The parameters σ_{LJ} and ϵ_{LJ}/k_B were taken from the NASA technical report[13] to be 4.320 Å and 121.0 K for CF_3 radical, to be 3.050 Å and 106.7 K for O atom, and to be 2.708 Å and 37.0 K for H atom, respectively. The calculation gives $k_{LJ}(CF_3 + O) = (1.0-1.4) \times 10^{-10}$ and $k_{LJ}(CF_3 + H) = (2.4-4.7) \times 10^{-10}$ cm^3 molecule^{-1} s^{-1} over the temperature range of 300−2500 K, which are much larger than the experimental results. The variational transition state theory[34,35] must be applied to discuss in more detail, but the relation between $CF_3 + O(^3P)$ and $CF_3 + H$ systems in the L−J collision rate coefficients is $k_{LJ}(CF_3 + H) > k_{LJ}(CF_3 + O)$ in agreement with the relation of the experimental rate coefficients, $k_{2c} > k_{1b}$.

The rate coefficients for the high-temperature $CH_3 + O(^3P)$ and $CH_3 + H$ reactions have already been determined by numerous workers. The rate coefficients recommended by Tsang and Hampson[36] are shown with broken lines in Figures 8 and 9. Both O and H atoms have higher reactivities with CH_3 radicals than with CF_3 radicals. We are currently studying the kinetics of the high-temperature reactions of CHF_2 and CH_2F with $O(^3P)$ and H atoms to discuss the relation between the number of fluorine atoms in fluoromethyl radicals and the reactivities with O and H atoms.

In this work, we found the results that CF_3 radicals could react with H atoms more easily than with $O(^3P)$ atoms, differing from CH_3 radicals. In the practical combustion, the dominant channel of CF_3 consumption is estimated to be the reaction with H atoms but not $O(^3P)$ atoms. Such difference in relative reactivity between CF_3 and CH_3 radicals can be explained as follows. For the $CF_3 + H$ reaction, the three-centered elimination of HF from CHF_3* is the main channel. In contrast, the elimination of H_2 from CH_4* cannot energetically occur for the $CH_3 + H$ reaction, so that the possible products of CH_4* are either $CH_3 + H$ or CH_4. As the former channel means the reverse reaction, it decreases the apparent rate coefficient for the $CH_3 + H$ reaction, leading to the result that $k(CH_3 + O) > k(CH_3 + H)$. This consideration is confirmed from the fact that the relation of the L−J collision rate coefficients is $k_{LJ}(CH_3 + H) > k_{LJ}(CH_3 + O)$ against the experimental data.

Conclusions

This study on kinetics of the high-temperature reactions of CF_3 with $O(^3P)$ and H atoms can be summarized as follows:

(a) The $CF_3 + O(^3P)$ and $CF_3 + H$ reactions proceed through F dissociation and HF elimination after their electrophilic additions, respectively.

(b) The rate coefficients for the reactions $CF_3 + O(^3P) \rightarrow CF_2O + F$ (1b) and $CF_3 + H \rightarrow CF_2(^1A_1) + HF$ (2c) were experimentally determined to be $k_{1b} = (2.55\pm0.23) \times 10^{-11}$ and $k_{2c} = (8.86\pm0.32) \times 10^{-11}$ cm^3 molecule^{-1} s^{-1} over the temperature ranges of 1900−2330 and 1150−1380 K, respectively. These results were in good agreement with some room-temperature data reported previously.

(c) From comparison of the rate coefficients, the dominant channel of CF_3 consumption in the combustion is estimated to be the reaction with H atoms, but not $O(^3P)$ atoms, differing from CH_3 consumption.

Acknowledgment. The authors wish to express our gratitude to Professor Frank Scott Howell S. J. for his valuable comments.

References and Notes

(1) Takahashi, K.; Yamamori, Y.; Inomata, T. *J. Phys. Chem. A* **1997**, *101*, 9105.
(2) Ryan, K. R.; Plumb, I. C. *J. Phys. Chem.* **1982**, *86*, 4678.
(3) Ryan, K. R.; Plumb, I. C. *Plasma Chem. Plasma Proc.* **1984**, *4*, 141.
(4) Tsai, C.; Belanger, S. M.; Kim, J. T.; Lord, J. R.; McFadden, D. L. *J. Phys. Chem.* **1989**, *93*, 1916.
(5) Tsai, C.; McFadden, D. L. *J. Phys. Chem.* **1989**, *93*, 2471.
(6) Biordi, J. C.; Lazzara, C. P.; Papp, J. F. *J. Phys. Chem.* **1976**, *80*, 1042.
(7) Takahashi, K.; Inoue, A.; Inomata, T. *Twentieth Symposium (International) on Shock Waves*; World Scientific: New Jersey, 1995; p 959.
(8) Gaussian 94W, Revision D.3; Frisch, M. J.; Trucks, G. W.; Schlegel, H. B.; Gill, P. M. W.; Johnson, B. G.; Robb, M. A.; Cheeseman, J. R.; Keith, T.; Petersson, G. A.; Montgomery, J. A.; Raghavachari, K.; Al-Laham, M. A.; Zakrzewski, V. G.; Ortiz, J. V.; Foresman, J. B.; Cioslowski, J.; Stefanov, B. B.; Nanayakkara, A.; Challacombe, M.; Peng, C. Y.; Ayala, P. Y.; Chen, W.; Wong, M. W.; Andres, J. L.; Replogle, E. S.; Gomperts, R.; Martin, R. L.; Fox, D. J.; Binkley, J. S.; Defrees, D. J.; Baker, J.; Stewart, J. P.; Head-Gordon, M.; Gonzalez, C.; Pople, J. A. Gaussian, Inc.: Pittsburgh, PA, 1995.
(9) Whitten, G. Z.; Rabinovitch, B. S. *J. Chem. Phys.* **1963**, *38*, 2466.
(10) Whitten, G. Z.; Rabinovitch, B. S. *J. Chem. Phys.* **1964**, *41*, 1883.
(11) Troe, J. *J. Chem. Phys.* **1977**, *66*, 4758.
(12) Gardiner, W. C., Jr.; Troe, J. In *Combustion Chemistry*; Gardiner, W. C. Jr., Ed.; Springer-Verlag: New York, 1984; p 173.
(13) Svehla, R. A. *NASA Technical Report R-132*, 1962.
(14) Cambi, R.; Cappelletti, G.; Liuti, G.; Pirani, F. *J. Chem. Phys.* **1991**, *95*, 1852.
(15) Foresman, J. B.; Frisch, M. J. *Exploring Chemistry with Electronic Structure Methods*, 2nd ed.; Gaussian, Inc.: Pittsburgh, PA, 1996; p 64.
(16) Sudbø, Aa. S.; Schulz, P. A.; Grant, E. R.; Shen, Y. R.; Lee, Y. T. *J. Chem. Phys.* **1979**, *70*, 912.
(17) Curtiss, L. A.; Raghavachari, K.; Pople, J. A. *J. Chem. Phys.* **1993**, *98*, 1293.
(18) Klatt, M.; Rohrig, M.; Wagner, H. Gg. *Ber. Bunsenges Phys. Chem.* **1991**, *95*, 1163.
(19) Thielen, K.; Roth, P. *Combust. Flame* **1987**, *69*, 141.
(20) Just, Th. In *Shock Waves in Chemistry*; Lifshitz, A. Ed.; Marcel Dekker: New York, 1981; p 279.
(21) Zaslonko, I. S.; Mukoseev, Yu. K.; Skorobogatov, G. A.; Khripun, V. K. *Kinet. Catal.* **1990**, *31*, 912.
(22) Dobychin, S. L.; Mashendzhinov, V. I.; Mishin, V. I.; Semenov, V. N.; Shpak, V. S. *Dokl. Phys. Chem.* **1990**, *312*, 494.
(23) Glanzer, K.; Maier, M.; Troe, J. *J. Phys. Chem.* **1980**, *84*, 1681.
(24) Westbrook C. K. *Nineteenth Symposium (International) on Combustion*; The Combustion Institute: Pittsburgh, PA, 1982; p 127.
(25) Hanson, R. K.; Salimian, S. In *Combustion Chemistry*; Gardiner, W. C., Jr., Ed.; Springer-Verlag: New York, 1984; p 361.
(26) Baulch, D. L.; Drysdale, D. D.; Duxbury, J.; Grant, S. J. *Evaluated Kinetic Data for High Temperature Reactions. Volume 3 Homogeneous Gas Phase Reactions of the O_2-O_3 System, the CO-O_2-H_2 System, and of Sulphur-containing Species*; Butterworths: London, 1976; p 33.
(27) Morris, R. A.; Donohue, K.; McFadden, D. L. *J. Phys. Chem.* **1989**, *93*, 1358.
(28) Okada, K. Master Thesis; Sophia University, 1996.
(29) Miller, J. A.; Bowman, C. T. *Prog. Energy Combust. Sci.* **1989**, *15*, 287.
(30) Kee, R. J.; Rupley, F. M.; Miller, J. A. *Chemkin-II: A Fortran Chemical Kinetics Package for the Analysis of Gas-Phase Chemical*

Kinetics; Sandia National Laboratories Report SAND89-8009; Sandia Laboratories: Albuquerque, NM, 1993.

(31) Lutz, A. E.; Kee, R. J.; Miller, J. A. *SENKIN: A Fortran Program for Predicting Homogeneous Gas Phase Chemical Kinetics with Sensitivity Analysis*; Sandia National Laboratories Report SAND87-8248; Sandia Laboratories: Albuquerque, NM, 1991.

(32) Tsang, W.; Herron, J. T. *J. Phys. Chem. Ref. Data* **1991**, *20*, 609.

(33) Hirschfelder, J. O.; Curtis, C. F.; Bird, R. B. *Molecular Theory of Gases and Liquids*; Wiley: New York, 1966.

(34) Wardlaw, D. M.; Marcus, R. A. *J. Chem. Phys.* **1985**, *83*, 3462.

(35) Hase, W. L.; Mondro, S. L.; Duchovic, R. J.; Hirst, D. M. *J. Am. Chem. Soc.* **1987**, *109*, 2916.

(36) Tsang, W.; Hampson, R. F. *J. Phys. Chem. Ref. Data* **1986**, *15*, 1087.